Journal of South American Earth Sciences 52 (2014) 57–71

Contents lists available at ScienceDirect

Journal of South American Earth Sciences

journal homepage: www.elsevier.com/locate/jsames

Geophysical structures and tectonic evolution of the southern Guyana shield, Brazil

João Willy Corrêa Rosa*, José Wilson Corrêa Rosa, Reinhardt A. Fuck

Instituto de Geociências, Universidade de Brasília, Campus Universitário Darcy Ribeiro, 70910-900 Brasília, DF, Brazil

ARTICLE INFO

Article history:
Received 7 April 2013
Accepted 11 February 2014

Keywords:
Guyana shield
Amazonian craton
Aerogeophysical survey
Proterozoic terrains
Seismic anisotropy
Shear-wave splitting

ABSTRACT

Aerogeophysical data of an area located on the southern portion of the Guyana shield in Brazil was processed using a fine interpolating mesh, and a corresponding spatial data integration strategy which included the stacking of different high-resolution images, and interpretation following quality control of these. The selected images were correlated to the local known surface geologic units, and to the spatial distribution of the main geochronological provinces of the Amazonian craton. The interpretation of the results also included the available geophysical information for the region, related to Moho depth values, and previously determined SKS shear-wave splitting direction. The observed magnetic regional trends may be strongly influenced by the Proterozoic crustal structure in the area, while radiometric anomalies correlate with the more detailed geologic features. Based on the parallelism among mapped geochronological provinces of the Amazonian craton, and observed geophysical structures on the study area, a geotectonic model is proposed for southern Guyana shield at Proterozoic age.

1. Introduction

Considering what is currently known about Precambrian shields (*e.g.* Ernst, 2009; Sleep and Windley, 1982; Van Kranendonk, 2010) or summarized in geology textbooks (Prothero and Dott, 2009; Hamblin and Christiansen, 1998), these units form the core of present-day continents. Shields are currently geologically stable areas, consisting of smaller Archean cratons welded together and surrounded by Proterozoic former orogen areas. Archean cratons are composed of two types of rocks: granite-gneiss terrains, which represent the primitive continents, and older or younger greenstone belts, which represent the primitive oceans (Prothero and Dott, 2009). The Archean granite-gneiss rocks are sodium-rich, indicating a greater mantle source than later potassium-rich granites, while the greenstone belts contain mostly ultramafic volcanic rocks. The latter represent the result of total melting of the upper mantle, and are only found in Archean rock units. Other rock units found in greenstone belts include rock types that resulted from partial melting of the mantle, from the differentiation of magma, or from the erosion of older crustal rocks. Archean cratons probably formed by the collision of granite-gneiss micro-continents with portions of primitive greenstone oceans trapped along sutures. Intense mantle convection, with small convection cells, and small plates with thin lithosphere, were the main characteristics of Archean plate tectonics (Prothero and Dott, 2009).

The final consequence of Proterozoic plate tectonics was the consolidation of the former small plates into large stable cartons. At this point, South America was part of the western portion of Gondwana. On the subsequent Proterozoic crustal evolution (Prothero and Dott, 2009), it is well-known that it was dominated by Wilson cycles, with the rifting of the former larger continents into small fragments, followed by the dispersal and subsequent consolidation of the continental crust into supercontinents. During the Early Proterozoic, it is known that the Wilson Cycle was already active, with rifting and subsequent suturing along the margins of the Archean provinces The geologic structure of continents and their margins were subsequently influenced by the Precambrian tectonics events described above.

As a summary of the Precambrian evolution of the continents, the current knowledge (Prothero and Dott, 2009) is that, while Archean proto-continents measured 100–500 km in width, Proterozoic continents measured from 1000 to 2000 km in width. These estimates of early continental sizes compare with the current 5000 to 10,000 km in width of present-time continents on Earth.

In this work, we consider an area located south of the Guyana shield (Fig. 1). The first effort of our group in this area was the installation of the IRIS Pitinga (PTGA) seismological station (Rosa, 1993). The study area was later surveyed by a temporary

* Corresponding author.
E-mail address: jwilly@unb.br (J.W.C. Rosa).

http://dx.doi.org/10.1016/j.jsames.2014.02.006

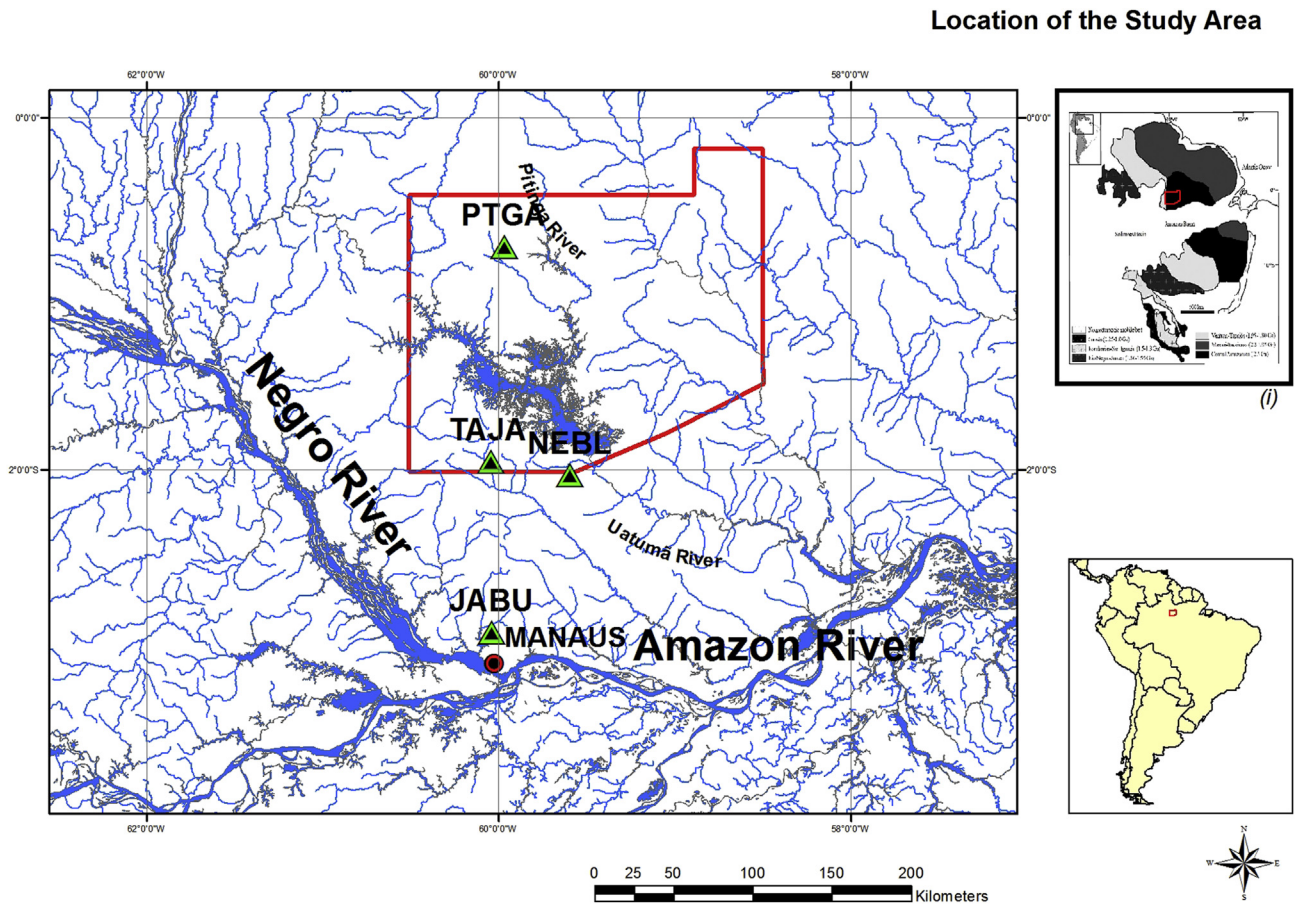

Fig. 1. Location of the study area. The location and code of each of the four seismological stations of Krüger et al. (2002) (PTGA: Pitinga, TAJA: Tajá, NEBL: Neblina, and JABU: Jabuti), as well as the city of Manaus, and some rivers, are shown. The red line limits the aerogeophysical survey area. *(i)* Geochronological provinces of the Amazonian craton (from Valério et al., 2012). (For interpretation of the references to color in this figure legend, the reader is referred to the web version of this article.)

seismological experiment from March 1997 to September 1998 using three broadband seismological stations together with the PTGA station (Krüger et al., 2002). The survey included the application of the receiver function technique to determine the crustal structure, using P-S converted waves and multiple reflections at crustal internal discontinuities. That study also included the analysis of the polarization of SKS waves to determine splitting times and fast directions of observed anisotropy.

The present work includes the processing and interpretation of the newly available aerogeophysical data (CPRM, 2007), with subsequent spatial data analysis using GIS techniques (combining both geophysical and geological information). The objective is to contribute to the better understanding of the Proterozoic terrains found in the study area.

2. Geological setting

The historical lack of geologic information in the Amazon region is related to both its sparse population, and the lack of rock outcrops, due to the dense tropical forest coverage, and corresponding thick soil layers. On the other hand, the Amazonian craton displays one of the most complete sequences recording Archean-Proterozoic crustal evolution on earth (Valério et al., 2009). This is related to the almost unique case of well-preserved rocks from both eons in its basement and volcanic-sedimentary cover (Almeida et al., 2000; Brito Neves and Almeida, 2003).

So, despite the mentioned environmental and logistical difficulties, which limit the available knowledge, some models of geologic evolution for the Guyana shield, and for the craton as a whole, were proposed: Santos et al. (2000, 2004); Tassinari and Macambira (1999, 2004). In the specific case of the geological evolution of the southern Guyana shield, we have contributions from Costi (2000), Costi et al. (2000), Fraga (2002), Fraga et al. (2009a, 2009b), Almeida (2006), Almeida et al. (2007, 2008), Ferron (2006), Ferron et al. (2006, 2010), Valério et al. (2009, 2012). There has been a constant effort to review the proposed division of the Amazonian craton into different units. The available information of the two past decades (namely, new regional geologic maps, geochronological dating based on Sm–Nd, Pb–Pb, and U–Pb methods, and now aerogeophysical surveys) has allowed geologists to group in two main proposals. The two proposed divisions of the Amazonian craton into geochronological units (insert on Fig. 1) include the evolution throughout orogenic cycles, of its crustal layer, including the accretional processes and tectonic deformation processes (Tassinari and Macambira, 1999, 2004; Santos et al., 2000, 2001; Santos, 2003).

When we consider the specific case of the region studied in this work, from its known geologic history, we notice that it includes important outcrops that tell us much from important magmatic events, which are part of the Guyana shield, Paleozoic to Cenozoic sedimentary rocks, from the Amazon basin, as well as Cenozoic records of sedimentary deposits and late soils, and Cenozoic tectonic processes (Souza and Nogueira, 2009). The area is crossed by an important highway, namely BR-174, which offers many road cuts with outcrops that furnish important data for the geologic history of the area. The geologic environment of the area includes

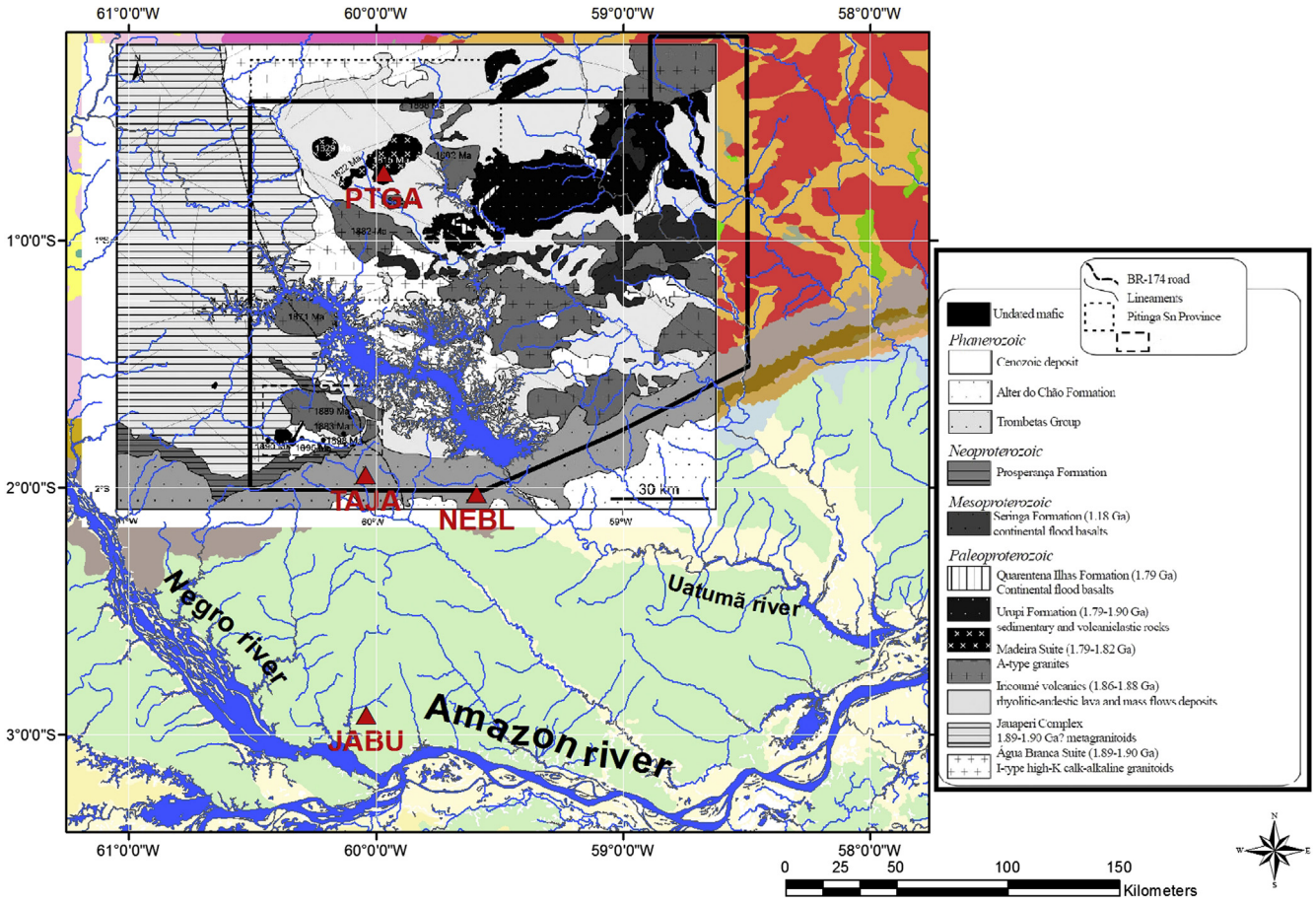

Fig. 2. Regional geological map of the study region, including the southern part of the Guyana shield, compiled from Bizzi et al. (2003) in the background (colored), stacked by a recent Pitinga region geologic map with its corresponding legend (from Valério et al., 2012). Also shown are the geographical location of the four seismological stations, and the limits of the aerogeophysical survey area. (For interpretation of the references to color in this figure legend, the reader is referred to the web version of this article.)

the northern border of the Paleozoic Amazon basin and the southern portion of the Guyana shield, basement to the basin in this area (Souza and Nogueira, 2009). The Proterozoic granitic and volcanic rocks are part of the Tapajós-Parima province, based on the proposed division of Santos et al. (2000, 2001), and Santos (2003), which evolution included the accretion of successive magmatic arcs during 2.10 to 1.87 Ga, and which were added to the Amazonia Central province, the Archean core of the Amazonian craton.

Based on geologic and geochronological data, Santos et al. (2001) and Santos (2003) proposed to separate the Tapajós-Parima province into the Alta Floresta, Tapajós (Lamarão et al., 2002, 2005), Waimiri, and Parima domains. Taking into account this division of the Tapajós-Parima province, the area we consider in this work would be part of the Waimiri domain, which rocks are, in large areas, covered by thick Phanerozoic marine to fluvial sedimentary rock layers. The Waimiri domain rocks show strong genetic and geochronological similarities with rocks from the Tapajós domain (Lamarão et al., 2002, 2005), but show only slight similarities with rocks from the Alta Floresta and Parima domains. Correlation between the Tapajós domain with the southern Guyana shield was established by Almeida et al. (2007). Santos et al. (2006) later named Matupá the originally selected Alta Floresta domain designation, and proposed an eastern extension of the original Tapajós-Parima province. This is the model used by Bizzi et al. (2003) for the Amazon region, and considered in further work developed by CPRM in some other maps (Fig. 2).

On another model, Valério et al. (2009), Tassinari and Macambira (1999, 2004), and Tassinari et al. (2000) proposed that the Amazonian craton is formed of the following geochronological provinces: an Archean core, represented by the Amazonia Central Province (older than 2.5 Ga), surrounded by mobile belts, namely the Maroni-Itacaiunas (2.2–1.95 Ga), the Ventuari-Tapajós (1.95–1.85 Ga), the Rio Negro-Juruena (1.85–1.55 Ga), the Rondoniana-San Ignácio (1.5–1.3 Ga), and the Sunsás (1.24–1.0 Ga) provinces.

Following Valério et al. (2009) on a more recent review, evidence of crustal evolution in the Amazonian craton seems to suggest that the development of the Ventuari-Tapajós, and of the Rio Negro-Juruena provinces, as well as part of the Maroni-Itacaiunas, and of the Rondonian-San Ignácio provinces, began with the accretion of mantle material. On the other hand, the Sunsás Province, and part of both the Rondoniana-San Ignácio and the Maroni-Itacaiunas provinces seem to be related to a reworking process of older continental crust (Valério et al., 2009).

According to the previous work of Tassinari and Macambira (1999), Tassinari et al. (2000), and Valério et al. (2009), it is estimated that about 30 percent of the Amazonian craton was derived from the mantle during the Archean, while 70 percent of that craton was derived from the continental crust, which should also include contributions from accretion of mantle material during the Proterozoic.

The area of our study has been included in the southern Uatumã-Anauá domain (Uatumã subdomain), on the central sector of the Amazonian craton (Valério et al., 2005, 2006). The oldest

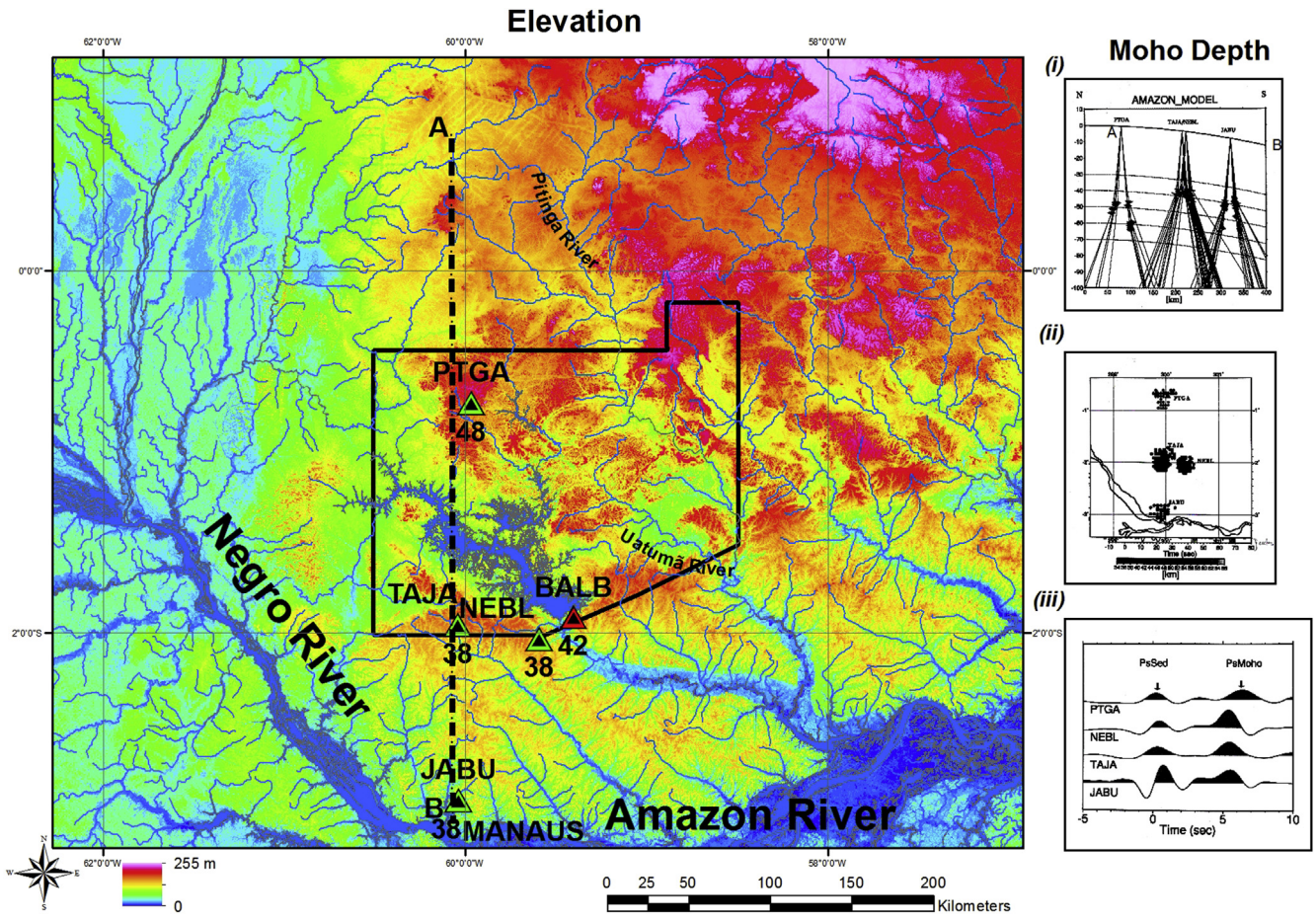

Fig. 3. Elevation of the study region, and Moho depth values for the area, including the results of Krüger et al. (2002) and the BALB (Balbina) station result of Lloyd et al. (2010). The black line limits the aerogeophysical survey area. The dashed line A-B indicated the N–S cross section across the study area for which we display the following results of Krüger et al. (2002): *(i)* Moho depth back-projection profile, obtained from ray-tracing on the Amazon crustal model for the study area. The horizontal discs mark the lateral and vertical extensions of the corresponding Fresnel zones. In this case, a modified IASP91 model (Kennett and Engdahl, 1990) was used; *(ii)* corresponding averaged Moho depth for the area; *(iii)* marked P-to-S conversions at the sediment/basement interface and at the Moho, from the stacked receiver function traces.

geologic units are two successive magmatic events, dated 1.90 and 1.81 Ga. The oldest of these two, the Água Branca syn-collisional I-type calc-alkaline suite, dated 1.90–1.89 Ga. The latest, a post-collisional to anorogenic A-type magmatism, represented by the Iricoumé-Mapuera volcanic-plutonism, dated 1.88–1.87 Ga, and the Moderna-Madeira granites, dated 1.82–1.81 Ga (Souza and Nogueira, 2009).

There are several geochronological data available for the studied area, all of them from Paleoproterozoic granitic, volcanic, and magmatic-derived metamorphic rocks (Araújo Neto and Moreira, 1976; Santos et al., 1997; Costi et al., 2000, 2009; Fuck et al., 1993; Santos et al., 2001; Reis et al., 2003; Bastos Neto et al., 2009; Ferron et al., 2006, 2010; Valério et al., 2009).

During the late Proterozoic, extensional tectonics prevailed in the region, and the Prosperança basin fluvial and coastal sedimentary deposits were created. In the early Paleozoic, a rift-syneclise phase occurred, generating the intracratonic Amazon basin, where thick coastal to marine sedimentary layers were deposited. These layers were then affected by glacial events. At the end of the Mesozoic era, a fluvial-lacustrine depositional system prevailed, and in the Cenozoic era, the region was affected by intense laterization/bauxitization events. Finally, the area was affected by transtensive neogene tectonic processes, with block uplift and downlift. This changed the relief, and produced colluvial and alluvial deposits (Souza and Nogueira, 2009).

3. Geophysical setting

3.1. Receiver function analysis and Moho depth

A modified version of the receiver function analysis (Langston, 1977, 1979; Vinnik, 1977; Kind and Vinnik, 1988; Yuan et al., 1997) was used by Krüger et al. (2002) to determine the crustal and upper mantle structure of our study area. In addition, a simple method, created by Zhu and Kanamori (2000) was used to estimate the crustal thickness and the average crustal Vp/Vs ratio (Fig. 3). The results of Krüger et al. (2002), displayed on map in Fig. 3, show an increase of the Moho depth from about 38 km near Manaus, located on the Amazon Basin, dipping north at an angle around 20°, to approximately 48 km depth, in the area where the PTGA station is located to the north of their study area. These results show that the crustal thickness value below PTGA is quite high, even for a shield area, with the observed upper mantle structure showing a gradual increase of the velocities at the Moho. We have also included in Fig. 3 the more recent result of Lloyd et al. (2010) for the Moho depth at the BALB (Balbina) seismological station. Krüger et al. (2002) point that a similar case, of comparable crustal thickness and the upper mantle velocity structure, was found in Scandinavia (Bungum et al., 1980; Mooney et al., 1998). In southeastern Brazil, James et al. (1993) found crustal thicknesses of about 40 km for Brazilian shield.

3.2. Transition zone discontinuities

For the case of the stacked, band-pass filtered (between 2 and 50 s) receiver function obtained for the study area, the results of Krüger et al. (2002) show that the corresponding 410 km anomaly would be at 408 km in the southern portion of the Guyana shield, while the 660 km anomaly would be at 656 km. The latter anomaly corresponds to the spinel to perovskite transition, while the former corresponds to the transition between olivine to spinel in the upper mantle (Grand and Helmberger, 1984). The results of Krüger et al. (2002) also indicated an upper mantle discontinuity at 521 km, corresponding to 55.5 s.

3.3. S-wave anisotropy analysis

Krüger et al. (2002) analyzed the polarization of SKS waves to determine anisotropy in the study region considered in this work. The resulting splitting times and fast directions of anisotropy of Krüger et al. (2002) show that the anisotropy can be represented by a fast direction oriented roughly 110° and an average splitting time of about 0.6. The observed splitting time is referred by Vinnik et al. (1992) as typical for a shield area. The resulting average symmetry axis direction is not parallel to the absolute plate motion of the South American plate. A very close result was obtained by Ivan et al. (2001), who examined a set of 35 waveforms of the PTGA station, and concluded that the fast wave direction of their SKS and SKKS results have a mean value of 101° ± 10°, with mean delay time of 1.04 ± 0.1 s Krüger et al. (2002), favor the frozen-in anisotropy hypothesis, related to past orogenies, summarized by Silver (1996), to explain the measurements for the area.

3.4. SRTM3 radar data

We have also considered the available Shuttle Radar Topography Mission (SRTM) digital data available for South America, sampled at three arc-seconds in latitude and longitude (SRTM3 data). Three arc-second data of South America were generated by averaging of the original one arc-second samples. In this case, we selected the images available for the region, which were added to a large image mosaic, and treated with equalization enhancement. A total of 96 SRTM3 images were used in order to build the mosaic necessary to the joint image processing of the aerogeophysical data considered in this work.

4. Material and methods

4.1. Aerogeophysical data

The released aerogeophysical survey for the area (CPRM, 2007) includes both aeromagnetic and aeroradiometry data, collected between January 12 and July 15, 2007. The study was planned to include an area previously uncovered by aeromagnetic surveys in Brazil. Three different aircraft were used in the survey, which covered a total area of 36,201 km^2, along data sampling flight line profiles totalling 73,427.27 km, added to 3840.25 km tie line total length. If we consider the compilation of magnetic data for South America of Fairhead and Maus (2003), or the compilation of data for the World Digital Magnetic Anomaly Map (Maus et al., 2007), we notice that the survey considered in this work fills a large previously existing gap on those databases.

The description of all sensors, recording and positioning equipment is summarized by CPRM (2007). The direction adopted for the survey flight lines was North-South, with 500 m spacing. The used tie flight line direction was East–West, with 10 km spacing. The sampling rate used was 0.1 s (magnetometer), and 1.0 s (spectrometer). Average flight height was 100 m. The average flight velocity for each of the three aircraft used was the following: 277 km/h, 281 km/h, and 288 km/h. Considering the flight velocity used for each of the three planes, the corresponding magnetometer sampling distance on the ground ranged between 4.0 and 7.8 m. The data were corrected using the current, standard procedures used in aeromagnetic data processing (Luyendyk, 1997) applied to the original data by the contractor (FUGRO Company), and all correction procedures were summarized in the survey report (CPRM, 2007), supplied to us with the corrected, geo-referenced data by CPRM, the Brazilian Geological Service.

For the aeroradiometric data, the data correction routine used followed the proposed procedures of airborne gamma ray spectrometer surveying of the International Atomic Energy Agency (IAEA, 1991). The corrections applied first included the series processing, where the live time was considered for the transformation of the unprocessed data corresponding to the measured total count, K, U, Th, and upward U channels into values of count per second of each of these channels (IAEA, 2003). Other data correction to the radiometric data applied by the contractor are summarized in the project report (CPRM, 2007). Accordingly, the radiometric data were also all corrected for possible effects of topographic changes along the aircraft paths. The objective of this procedure was to normalize all aeroradiometric readings into the standard flight height value of 100 m, in order to eliminate possible false anomalies related to topographic highs.

4.2. Data processing

For this work, we took the original grid values of the survey, and applied a kriging interpolation routine available from the Oasis Montaj software package of the Geosoft system. In this case, we used an interpolation grid measuring 125 by 125 m. Kriging is a statistical gridding technique for random data, non-parallel line data or orthogonal line data. The latter is the case of our work. We found that, using kriging, which could even treat data that were randomly sampled in the area, and which would give a random appearance when plotted, would be the most appropriate interpolating technique to be applied to generate our final gridded data maps from the field sampled data. The routine used for this first calculates a variogram of the data, which shows the correlation of the data as a function of distance (Geosoft, 2010). The computed variogram enables to select a model that best defines the variance of the data. The selected model enables the kriging technique to estimate the data values at the nodes of the desired interpolation grid. The routine used for the kriging technique supports ordinary kriging, as well as universal kriging. The latter allows the data to contain a regional trend (Journel and Huijbregts, 1978). In the case of the kriging routine used, it includes the application of a de-aliasing filter and both linear and logarithmic griding options.

Following the processing steps, the maps generated by interpolation were first compared with the known geologic data base, and to the available radar SRTM3 data (which enables us to consider an independent digital terrain model). An example of the digital image processing and corresponding spatial data integration strategy is shown on Fig. 4, where we present the stacking of different sources of data. The added control of the proper color palette, contrast, shading, brightness, to the stacking effects, were used to visually select the images which we subjectively judged best showed the known geologic features of the study area.

5. Results

The aerogeophysical contour maps (*e.g.* Figs. 5–10) from the resulting application of the kriging interpolation were then

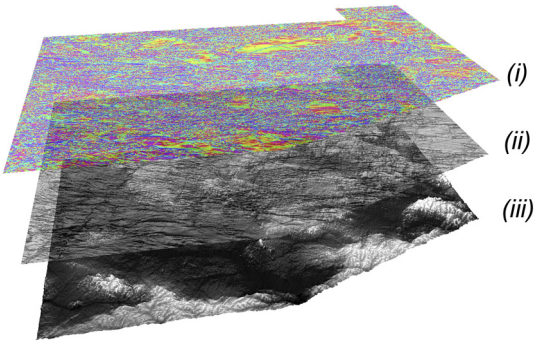

Fig. 4. Example of the digital image processing, and corresponding spatial data integration strategy, used in the stacking scheme for the different sources of data. Added control of the proper color palettes, contrast, shading, brightness, were used to enhance the stacking effects. (For interpretation of the references to color in this figure legend, the reader is referred to the web version of this article.)

processed using the image stacking strategy, which included the visual quality control and interpretation of the images. For all resulting maps presented here, we included the results of both SKS analysis of Krüger et al. (2002) for the Pitinga (PTGA), Tajá (TAJA), and Neblina (NEBL) seismological stations, as well as the NUVEL-1 model computed current plate motion vectors of the Nazca and South America plates.

In the first step of the analysis, we selected areas where some clear geologic structures could be used to verify the match between the aerogeophysical data and the mapped borders of the given known geologic structures. From Fig. 5, where we used the observed aeromagnetic anomalies, added to the gray-shaded aeromagnetic data, it is clear that the main granite bodies, as well as the syncline structure, located on the central-northern portion of the study area, are both well constrained. A sharp change on the main direction of the observed magnetic anomalies changed from EW direction, prevailing on the central and eastern portion of the image to an approximate N120E direction on the southwestern corner. The two image sections were separated using the marked dashed orange line (Fig. 5). So, the processing of the aeromagnetic data corrected to the IGRF with the proper gray scale (Fig. 5) allowed us to resolve the question of regional lateral heterogeneities and their prevailing lateral alignment.

In Fig. 6, we show the results of the total radiometric count for the area. We again use the scheme of plotting the SKS results of Krüger et al. (2002), as well as the NUVEL-1 model current plate motion vectors of the Nazca and of the South America plates (we also included this information on the other results of radiometric data). In the specific case of Fig. 6, the oldest geologic units visible on the image displayed are the rocks from the Iricoumé volcanics

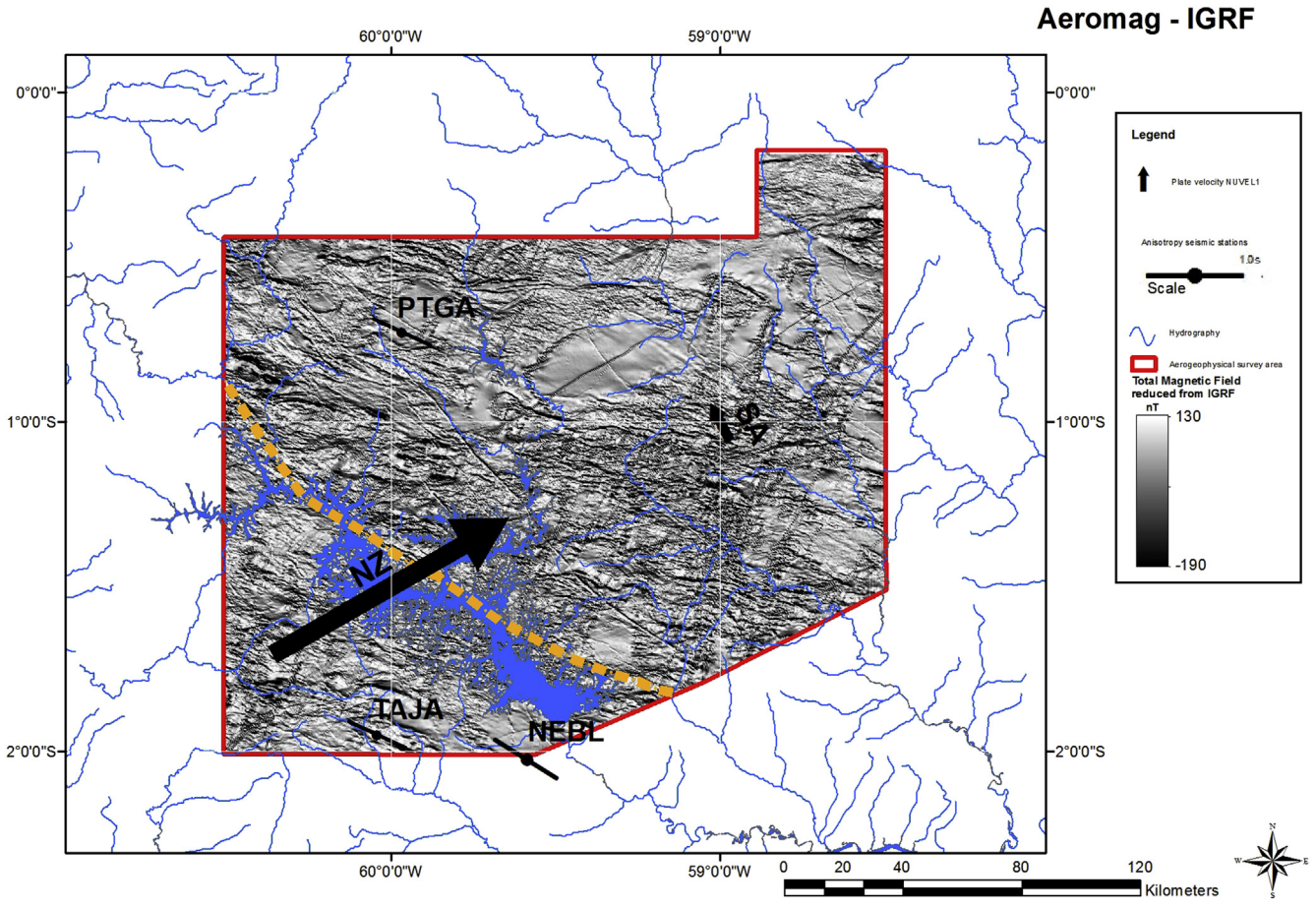

Fig. 5. Processed aeromagnetic anomalies (corrected for the IGRF), displayed using a grey scale with no shading, which was used for the processed image. On the foreground, the resulting direction of the SKS shear-wave anisotropy results of Krüger et al. (2002) are displayed, as well as the current day NUVEL-1 absolute plate motion vectors for both the Nazca (NZ) and South America (SA) plates. The dashed orange line corresponds to the interpreted border among the Central Amazon (>2.3 Ga) and the Ventuari-Tapajós (1.95–1.80 Ga) geochronological provinces of the Amazonian craton (Valério et al., 2012). (For interpretation of the references to color in this figure legend, the reader is referred to the web version of this article.)

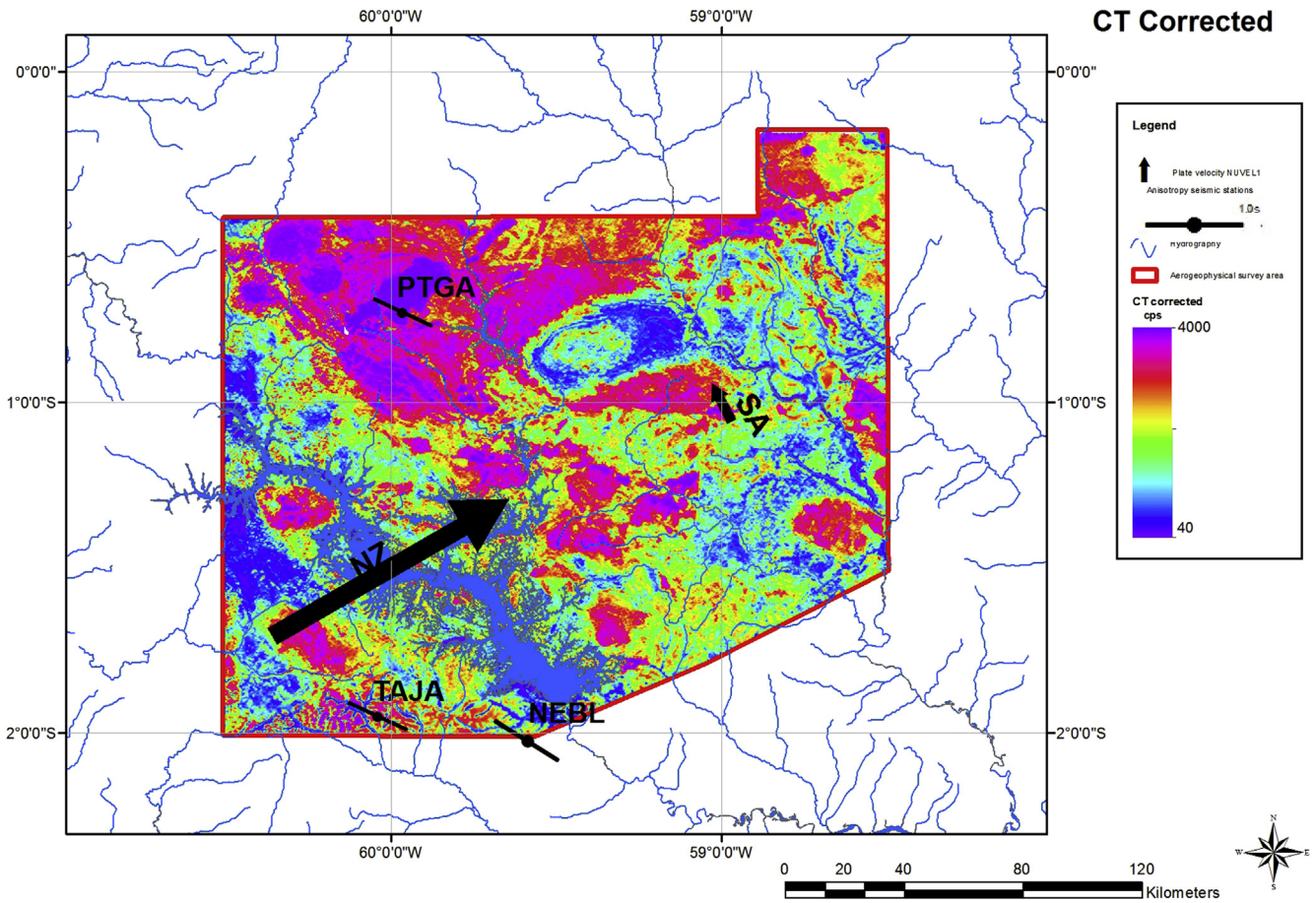

Fig. 6. Processed image showing the corrected total count radiation. On the foreground, the resulting direction of the SKS shear-wave anisotropy results of Krüger et al. (2002) are displayed, as well as the current day NUVEL-1 absolute plate motion vectors for both the Nazca (NZ) and South America (SA) plates.

and Mapuera granites (both included in the Uatumã Supergroup, 1.88 Ga, according to Ferron et al., 2006, 2010), which crop out in the region of the Pitinga mine. In the Pitinga mine area, the Madeira, Agua Branca, and Europa granites were also dated 1.83–1.82 Ga (Costi et al., 2000). We notice that the granite intrusions related to the Agua Branca Suite (1.95–1.90 Ga), of the work of Valério et al. (2006), and those mapped by Souza and Nogueira (2009) are all also very clear in the radiometric anomalies of Fig. 6. The Jauaperi suite metamorthic rocks (1.88–1.87 Ga), as well as the Mapuera granites, are also very clearly shown in the radiometric data of Fig. 6, and complete the set of the Paleoproterozoic rocks which crop out in the study area. From the Mesoproterozoic time, we can observe radiometric anomalies matching the outcrop of rocks from the Seringa Formation (1.08 Ga, according to Veiga et al., 1979), which crop out in a small area located in the central part of the study region, north of the Balbina reservoir (Fig. 6). From the Neoproterozoic time, we can match the radiometric anomalies related to the outcrops of the Prosperança Formation, located in a small portion south of the Balbina reservoir. Finally, the Phanerozoic rocks are represented in the study region by rocks from the Trombetas Group, as well as from the Alter do Chão Formation (Valério et al., 2006; Souza and Nogueira, 2009), found in the area located south of the Balbina reservoir, in the area corresponding to the Amazon sedimentary basin (Fig. 6). Some recent coluvio-alluvional deposits are also found in the study area, and were easily identified.

The individual contribution of the K corrected data is shown on Fig. 7, while the contribution of the U corrected data is displayed in Fig. 8. On Fig. 9, we present the distribution of the Th corrected data.

Examining Fig. 7, where the K corrected measured radiation values were displayed, we notice that the anomalies from the Iricuomé Group (1.96–1.90 Ga) are not as well defined as in Fig. 6. On the other hand, rocks from the Jauaperi Metamorphic Suite (1.88–1.87 Ga), and those of the Mapuera Intrusive Suite (1.87–1.81 Ga), which occur on the western portion of the study area (Valério et al., 2006), can be clearly separated on the map shown in Fig. 7, indicating that the K results show proper lateral resolution for these units.

If we consider the geological units from the Mesoproterozoic (*i.e.* from the Seringa Formation – approximately 1.08 Ga, according to Valério et al., 2006), known to outcrop in the area located south of the Pitinga mine, these can be also related to anomalies in Fig. 7. On the other hand, the Neoproterozoic rocks of the Prosperança Formation, which surface geology occurrence is restricted to a small area located south of the Balbina reservoir, are not clearly shown in the K anomaly map of Fig. 7. Finally, the border between the Precambrian shield and the Phanerozoic sedimentary rock units of the southern portion of the study area is very clear in Fig. 7.

On Fig. 8, where we display our resulting U radiation map, the anomalies are better correlated with the known surface geology features than those discussed in the previous results for the K radiation. For the Paleoproterozoic rock units of the Pitinga mine area, located on the central and eastern portions of Fig. 8, we see their corresponding, clear anomalies. In this case, all Paleoproterozoic rock units show a broad, red color characteristic anomaly,

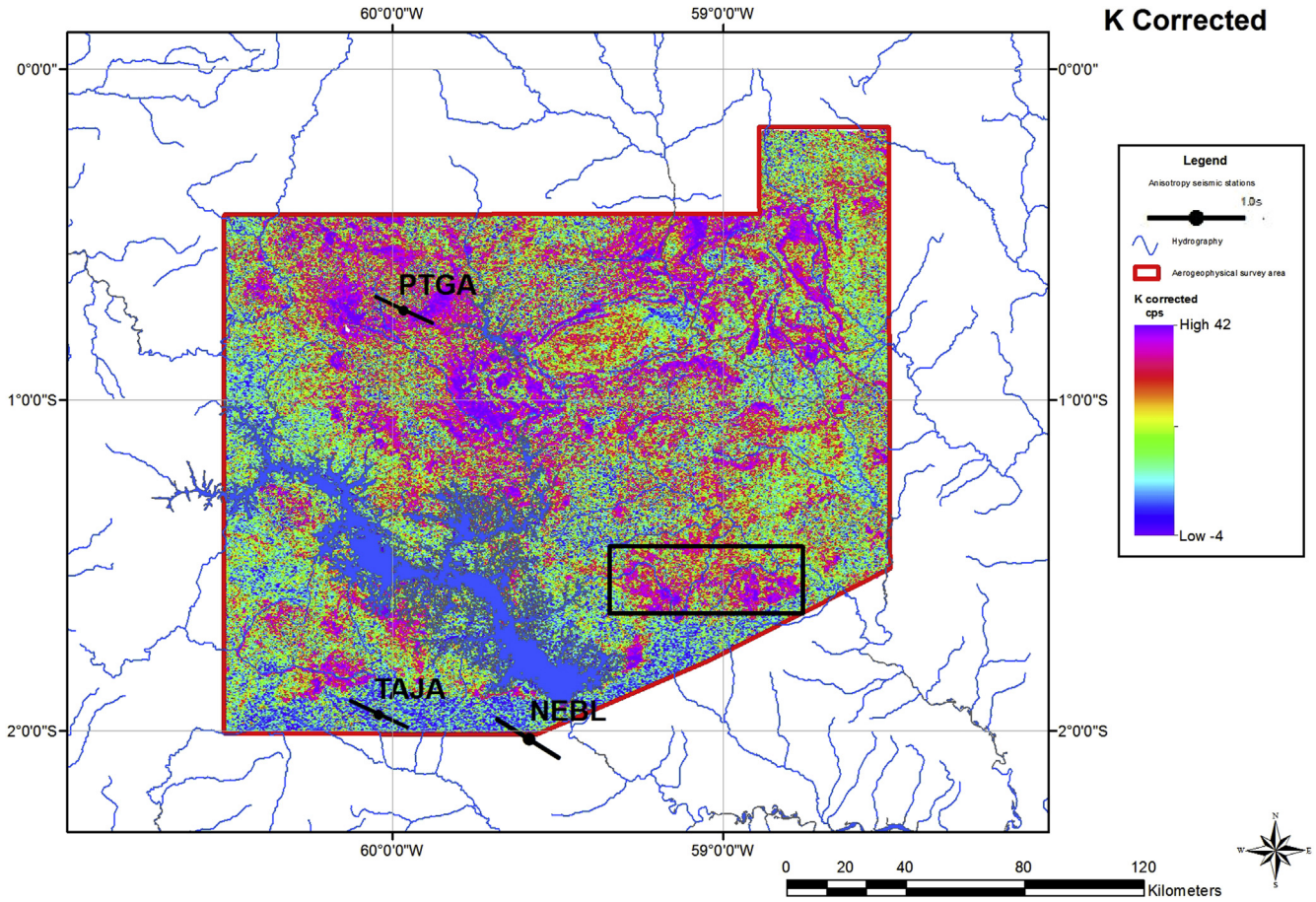

Fig. 7. Processed K radiation corrected data. On the foreground, the resulting direction of the SKS shear-wave anisotropy results of Krüger et al. (2002) are displayed, as well as the current day NUVEL-1 absolute plate motion vectors for both the Nazca (NZ) and South America (SA) plates. The marked rectangular area shows the anomalies identified as geological units from the Mesoproterozoic – Seringa Formation (~1.08 Ga, Valério et al., 2006).

limited to the east by the Pitinga reservoir and, further to the east, by the strong, clear, oval-shaped blue anomaly of the large syncline structure (Fig. 8). South of the syncline structure, we can see the fan-shaped red-colored anomaly along the Pitinga river valley, where strong radiation is associated with possible alluvial deposits possibly rich in tin ore, as well as in rare earth elements common in the mentioned Paleoproterozoic rocks of the Pitinga mine region. Both tin and rare earth elements are being mined in the Pitinga region for several decades now, and the downstream alluvial deposits may be related to these elements. It is also possible that this anomaly is due to the influence of granites or felsic volcanic rocks in the area.

The best pictured of the three radiometric components of the radiation field is the Th component result (Fig. 9). In this case, all major known geologic structures and rock units are clearly displayed. It is clear, from Fig. 9, that the stacked contribution of all three components (namely, K, U, and Th, displayed on the total count map of Fig. 9), demonstrates that the details are related to the contribution of the Th channel (Fig. 9). Considering the main geological units already discussed in this section, we can find on Fig. 9 the largest radiometric readings in the area of the Pitinga mine. For these strong anomalies, there is contribution from all Paleoproterozoic units present in this area: the Iricoumé Group, the intrusive granite suite Água Branca, the Jauaperi metamorphic suite, and the Mapuera instrusive suite. These terrains, which age range from 1.90 Ga to 1.81 Ga, are characterized by the large anomalies viewed in the large, broad area located north of the Balbina reservoir, and to the west of the large syncline structure located to the east of the Pitinga reservoir. It is also possible that the stronger positive radiometric anomalies reflect the influence of the Iricoumé volcanics and Mapuera and Madeira granite suites. The Madeira suite is particularly rich in radioactive elements. The opposite is true for the Agua Branca suite and maybe the Jauaperi metamorphic suite might also not be responsible for these positive anomalies.

In the Pitinga mine region limited by the rectangular area of Fig. 9, we notice that the Th component results, properly treated and interpreted, can help on the separation of the several granite bodies and other geologic units present in that part of the study area. The Pitinga mine region is characterized by a series of granite bodies and alluvial deposits that have been important for the exploration of tin ore present in the area. Most of what is known today from the intrusive suites related to the Proterozoic terrains of the southern Guyana shield are related to detailed mapping of these units on the past 30 years.

From the ternary diagram of the composed K–U–Th corrected radiation data, shown in Fig. 10, It is possible, using Fig. 10, to identify very narrow, and long, geologic sub-units and structures such as faults, in the long and broad, oval-shaped, syncline structure located on the north-central portion of the region of this study. This structure is known as the Pitinga syncline structure (Veiga et al., 1979, mapped this structure on a 1:1,000,000 scale), and it is known to include quartz-arcosean sandstone layers from the Urupi Formation (age around 1.88 Ga), stacked with pyroclastic

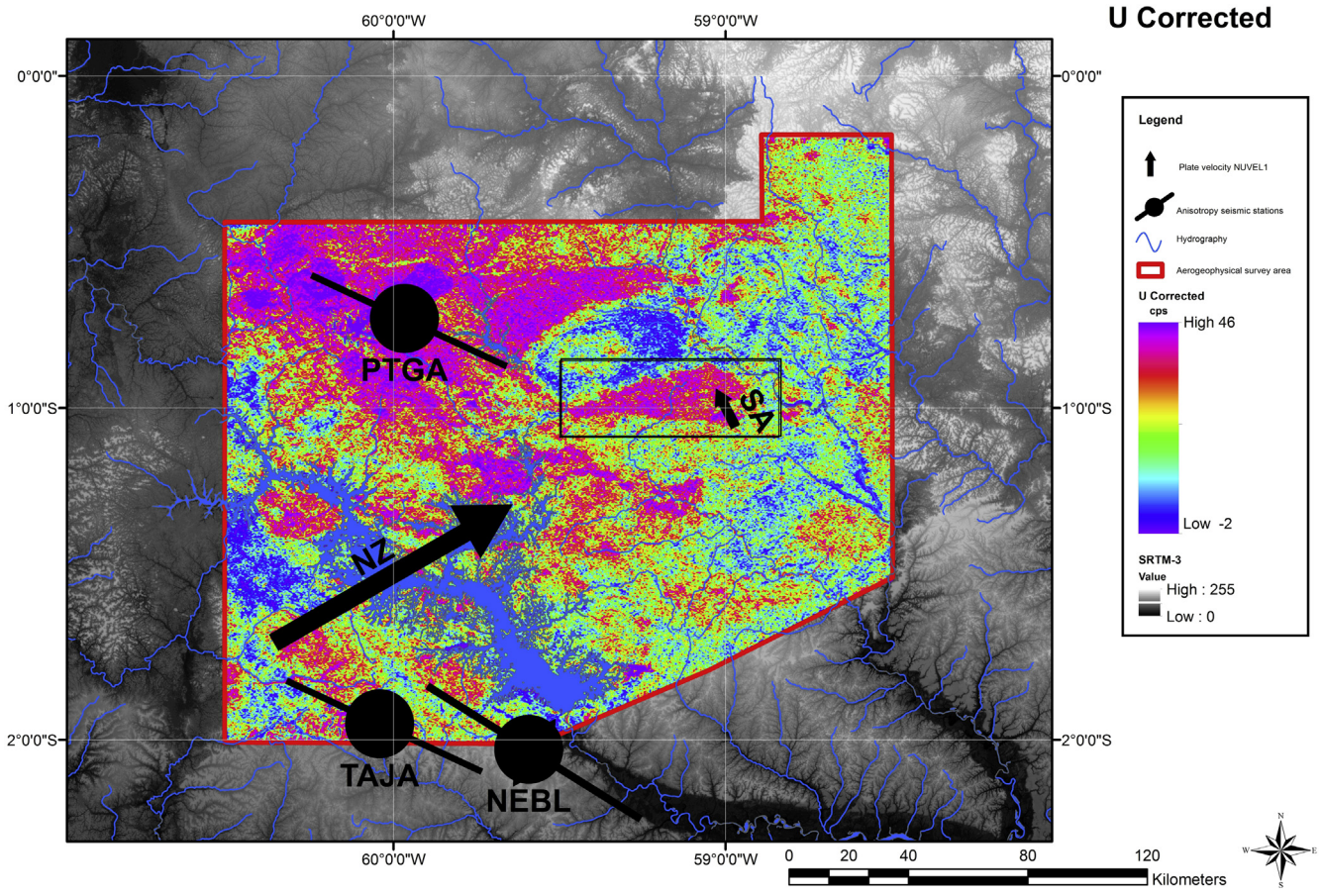

Fig. 8. Processed corrected U radiation, stacked to the radar SRTM3 data. On the foreground, the resulting direction of the SKS shear-wave anisotropy results of Krüger et al. (2002) and current NUVEL-1 absolute plate motion vectors for both the Nazca (NZ) and South America (SA) plates. Marked we point an area on the Pitinga river valley, where strong radiation is associated with possible alluvial deposits possibly rich in tin ore, and in rare-earth elements.

rock units (composed of tuff and ignimbrites) and sills of basic volcanic rocks (basalts, tholeiitic diabase units, from the 40 Ilhas Formation). There is an available 1780 ± 3 Ma SHRIMP age estimate for the diabase units of the area (Santos et al., 2002).

Anomalies which were moderately, or reasonably visible in some of the data bands we considered previously (Figs. 6–9), turn into highlighted new features, which lead into a better identification of some geologic features displayed on Fig. 10. We emphasize the changes observed along the southern border of the survey area, when moving northwards from the Phanerozoic Amazon sedimentary basin into the southern portions of the Guyana shield. The anomalies shown by the two rectangles located on the border of the Balbina lake, correspond to well-known granite intrusions (Valério et al., 2012).

6. Discussion

From the initial review presented in this work, it can be said that the geological knowledge on the southern part of the Guyana shield has improved much in the past few decades. Information from the most recent geologic regional data available for the area of our work (Fig. 2 – Valério et al., 2012) shows that we are considering terrains from the central portion of the Amazonian craton. The study area includes the exact western border of the Central Amazonian (>2.5 Ga), with its neighboring Ventuari-Tapajós (1.95–1.80 Ga) geochronological domains of that craton (Figs. 1 and 2). The previously known geophysical information on the area includes the Moho depth estimates on four different seismological stations installed on the Guyana shield and on its southern limit, in addition to a similar estimate near Manaus, located in the south of the area (Fig. 3). The Moho estimates, from the studies of Krüger et al. (2002) and Lloyd et al. (2010) indicate a Moho limit dipping around 20° to the north, accompanying the transition from the Amazon basin to the southern portion of the Guyana shield in the study area (Fig. 3 – inset ***i***).

Using the original regional aerogeophysical data (CPRM, 2007), kindly furnished to us by CPRM, we applied a series of digital image processing techniques, corresponding to a spatial data integration strategy, an example from which is shown on Fig. 4. The details of the image processing and generation of the final results have been reviewed, and examples shown on the previous section. What follows here is a discussion on what we believe would be our contribution on the treatment on such detailed data as the one provided by CPRM. The enhancement of the graphical features observed in the maps after the digital image processing was applied depends on many variables. The images presented on Fig. 5 for the aeromagnetometry results, and on Figs. 6–9 (corresponding, respectively, to the total count, and on K, U, and Th counts) for the radiometric results, are a summary of the ones which we considered more significant from the processing. From these, it is clear what is known about aerogeophysical survey data: the magnetic data are most useful for linear, and regional features, specially the ones involving changes related to major geologic or geochronologic units. This is clear on the marked border between the two geochronological provinces on Fig. 5. On the other hand, it is known that radiometric data yield, if properly treated, image contrasts

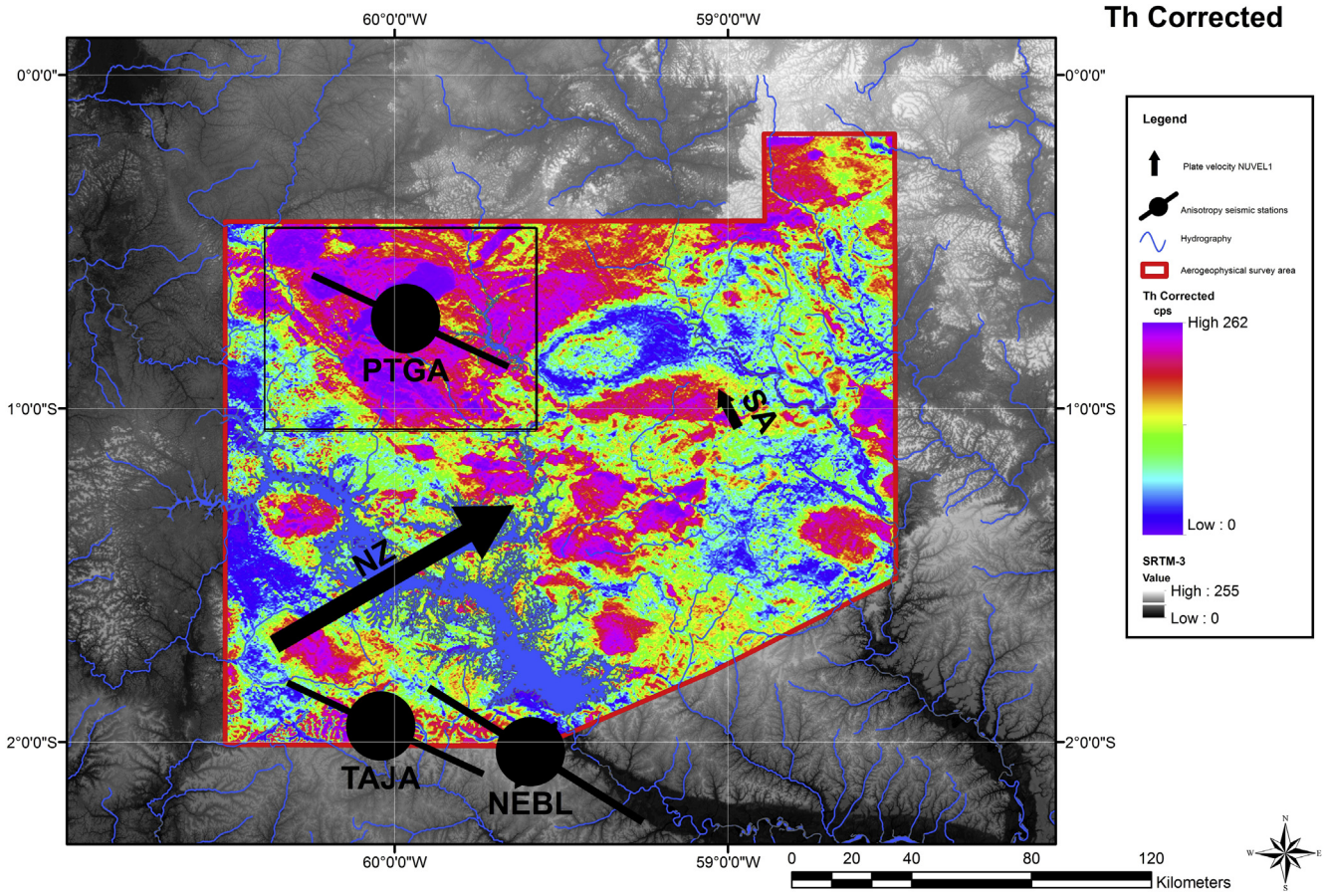

Fig. 9. Resulting corrected Th radiation, stacked to the radar SRTM3 image, with the measured direction of the SKS shear-wave anisotropy of Krüger et al. (2002), and the current day NUVEL-1 absolute plate motion vectors for both the Nazca (NZ) and South America (SA) plates. Marked area shows the Pitinga mine region.

related to some geologic details on shield features (*e.g.* granitic bodies). These contrasts were observed on Figs. 6–10, which includes the Ternary composed K–U–Th result of Fig. 10.

Combining the aerogeophysical interpolated data with SRTM-3 data proved to be very useful on enhancing some known geologic features (*e.g.* Figs. 8 and 9). This was performed using those radar data stacked to the processed magnetometric or radiometric images. Subjectivity is added when we consider that the stacking procedure was followed manually, while treating the proper light contrast, selected color palette, or shading effect applied to the process (Fig. 4).

On Fig. 11, we present another resource applied to the treated aeromagnetic data. In this case, we used the topographic image corresponding to the aerogeophysical original data provided by the contractor to CPRM (2007), to generate a DEM-digital elevation map. The treated aeromagnetic image was then stacked to the DEM. An additional resource was applied to the resulting surface of Fig. 11, allowing the 3-D surface to be rotated. This is a routine resource applied to interpret, for example, aero-photos. The rotated surface shown on Fig. 11, viewed from the SW towards the NE direction was the one we chose while changing the viewing angle. It displays the change in direction of the aeromagnetic anomalies of Fig. 5 from a normal angle to the orange dashed line, which was identified as the border among the two Amazonian craton geochronological units of Tassinari and Macambira (2004): the Amazonia Central Province (>2.3 Ga), and the Ventuari-Tapajós (1.95–1.80 Ga). While observing Figs. 5 and 11, it is possible to notice that the border limiting these two units follow the original valley of the Uatumã river, which was dammed to form the Balbina reservoir. This border is close to the border among the two units found on the most recent regional geologic map (viewed on Fig. 2, from Valério et al., 2009).

Based on our aeromagnetic results (Figs. 5 and 11), and previously available seismological information for the study area, we now address the observed change on main direction of the aerogeophysical anomalies, related to the geochronological units found in the study area. As pointed out in the previous section, the direction of the anomalies change on the interpreted dashed orange line, from EW, observed in the eastern and northern sections of Fig. 5, to approximately N120 E, observed in the southwestern corner of that image.

Silver and Kaneshima (1993), and later, Barruol et al. (1997), have already observed, for the splitting results obtained at stations located on the Superior province and on the midcontinental rift of the Canadian shield, that the fast split shear wave polarization direction is parallel to the local tectonic fabric. Bokelmann and Wüstefeld (2009) compared regional magnetic anomalies and seismic anisotropy results obtained from stations located on the North American craton. More recently, Wüstefeld et al. (2010), found on the East European craton a good correlation between anisotropy and regional magnetic field anomalies. In the eastern border of the Amazonian craton, Rosa et al. (2012) have compared aeromagnetic anomalies with the anisotropy direction derived from SKS seismological results.

The main anisotropy direction from seismological records was determined in the area by Krüger et al. (2002) (Table 1, Fig. 12). It

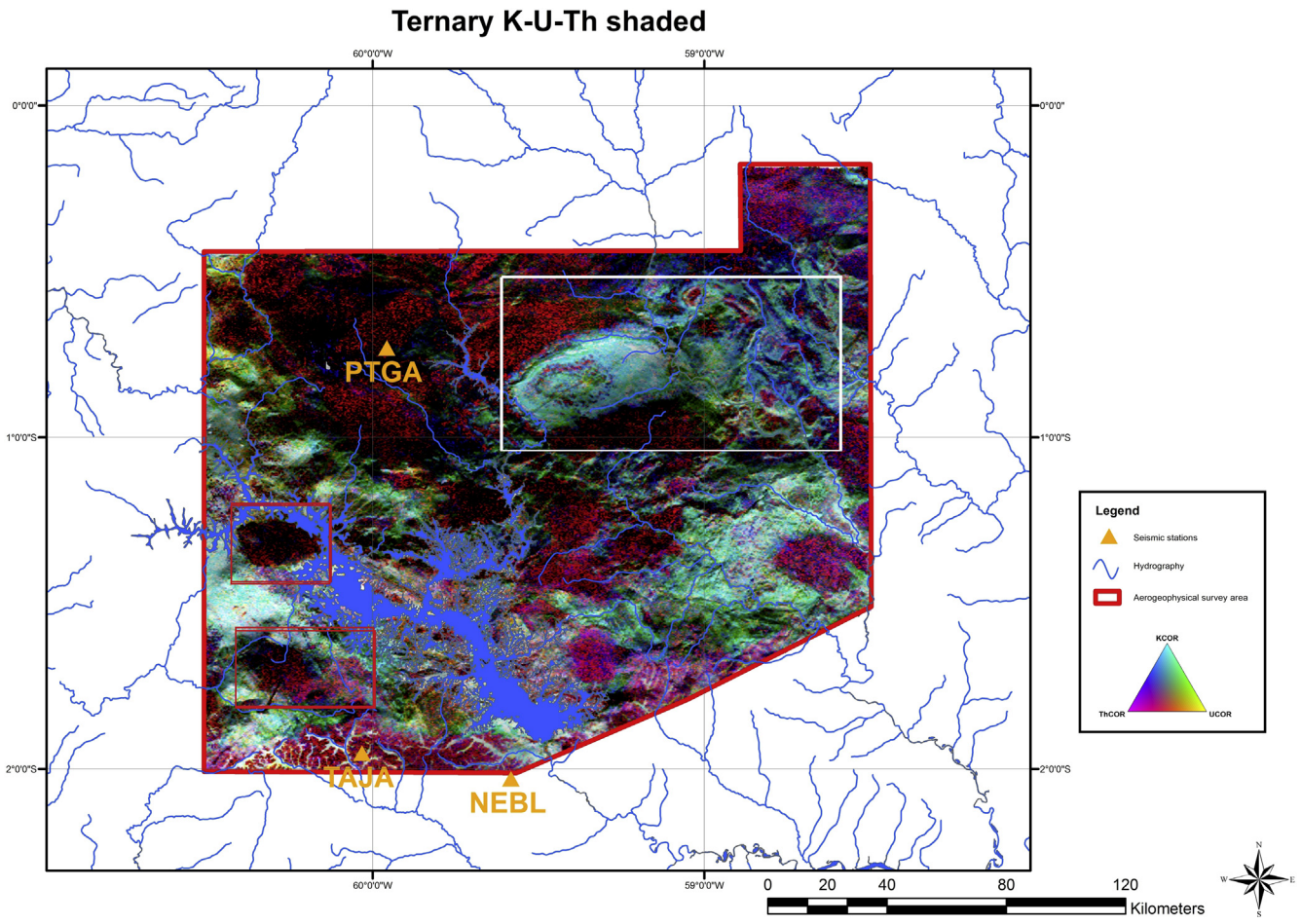

Fig. 10. Ternary composed K–U–Th corrected radiation diagram, and the regional hydrography data. On the foreground, we can observe the position of the seismological stations. The white rectangle shows the Pitinga syncline structure (Veiga et al., 1979), while the two red rectangles on the W and SW borders of the area show granitic intrusions. (For interpretation of the references to color in this figure legend, the reader is referred to the web version of this article.)

matches the prevailing direction of the most ancient rock units of the Guyana shield in Brazil, located in the eastern portion of Fig. 12. In the eastern area of the Guyana shield segment in Brazil (Fig. 12), we find the Neoarchean 2.8–2.5 Ga Granulite complex, and the Paleoproterozoic 2.3–2.1 Ga Vila Nova and Serra Lombarda groups, basically composed of Greenstone-Granite belts, according to McReath and Faraco (2006). The prevailing NW–SE azimuthal direction of these geological units, with the special emphasis on the greenstone belt formations, which were originally linear features upon their formation, match the direction of the observed aeromagnetic anomaly trends of the study area (Figs. 5 and 11).

If we consider the fact that Ivan et al. (2001) obtained basically the same resulting direction for the anisotropy using the PTGA station data, and the fact that Barruol and Hoffmann (1999) also

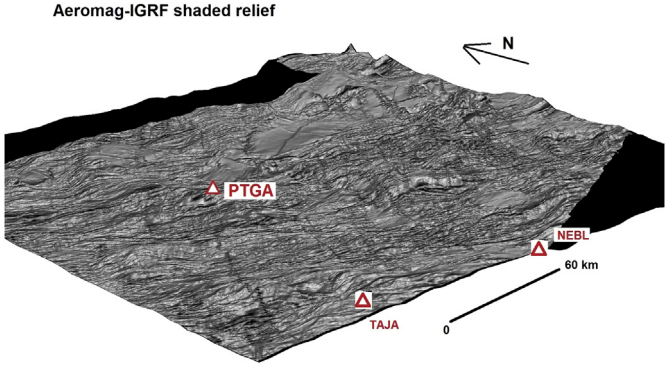

Fig. 11. Diagram with SW–NE relief view of the processed aeromagnetic data, corrected for the IGRF (same result displayed on Fig. 5), with shaded effect, on the observed topographic surface. The location of the three seismological stations located in the aerogeophysical survey area is displayed, as well as the approximate horizontal scale.

Table 1
Splitting Parameters for the Guyana shield.

Reference	Station	φ(o)	$d\varphi$(o)	δt(s)	$d\delta t$(s)	N
Barruol and Hoffmann (1999)	CAY (Cayenne)	119	5	0.69	0.05	8
	KOG (Kourou)	130	3	0.84	0.10	8
Ivan et al. (2001)	PTGA	101	10	1.04	0.1	35
Krüger et al. (2002)	PTGA	115	15	0.6	0.3	21
	TAJA	115	15	0.6	0.2	6
	NEBL	122	10.	0.7	0.1	8
	JABU	115	15.	0.6	0.2	15
Assumpção et al. (2011)	SNVB[a]	84	10	1.1	0.2	5

φ – average measured symmetry axis direction; $d\varphi$ is the corresponding standard deviation of the average.
δt – average splitting delay time; $d\delta t$ is the corresponding standard deviation of the average.
N – number of measurements (considering both SKS and SKKS results).
δt is the average splitting delay time – $d\delta t$ uncertainty (95% confidence limit); N is the number of measurements (considering SKS results).
[a] φ is the fast polarization direction, $d\varphi$ – uncertainty (95% confidence limit).

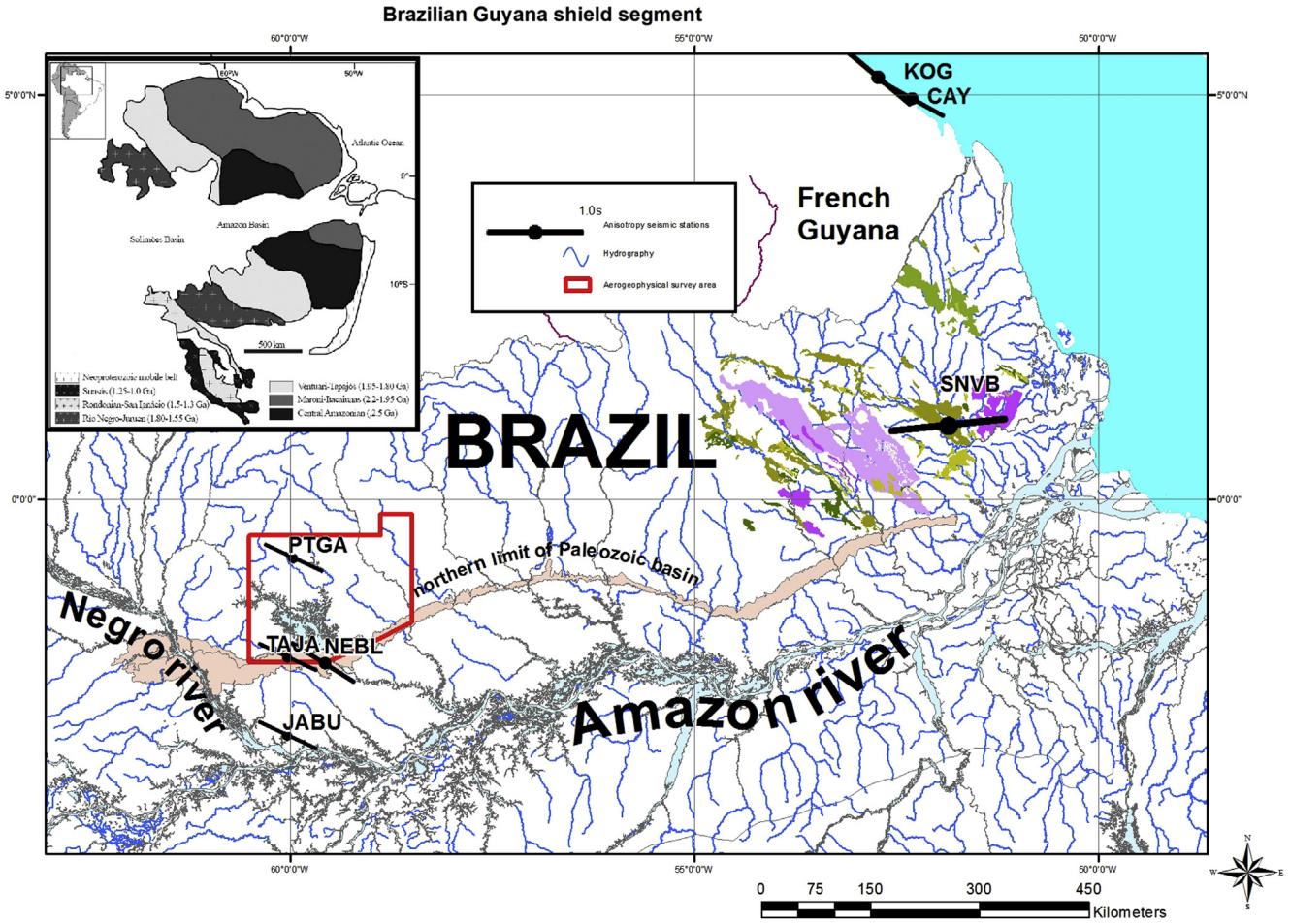

Fig. 12. Geologic map of the Brazilian segment of the Guyana shield. In this case, the aerogeophysical survey area, limited by the red border, and the location of the four seismological stations and the resulting direction of the SKS shear-wave anisotropy of Krüger et al. (2002). The oldest Phanerozoic known unit of the northern border of the Amazon basin (namely, the Paleozoic Trombetas Group, according to Bizzi et al., 2003) marks the southern border of the Guyana shield. Furthermore, the oldest known geologic units of the Guyana shield in Brazil are displayed on the west of the map (namely, the Neoarchean 2.8–2.5 Ga Granulite complex, and the Paleoproterozoic 2.3–2.1 Ga Vila Nova and Serra Lombarda Groups, basically composed of Greenstone-Granite belts, according to McReath and Faraco, 2006). Finally, we included the resulting direction of the SKS shear-wave anisotropy of the study of Barruol and Hoffmann (1999) for the two French Guyana stations (CAY-Cayenne and KOG-Kourou), and the result of one station (SNVB-Serra do Navio) from Assumpção et al. (2011). On the inset, we show the distribution of geochronological provinces on the Amazonian craton (from Valério et al., 2012). (For interpretation of the references to color in this figure legend, the reader is referred to the web version of this article.)

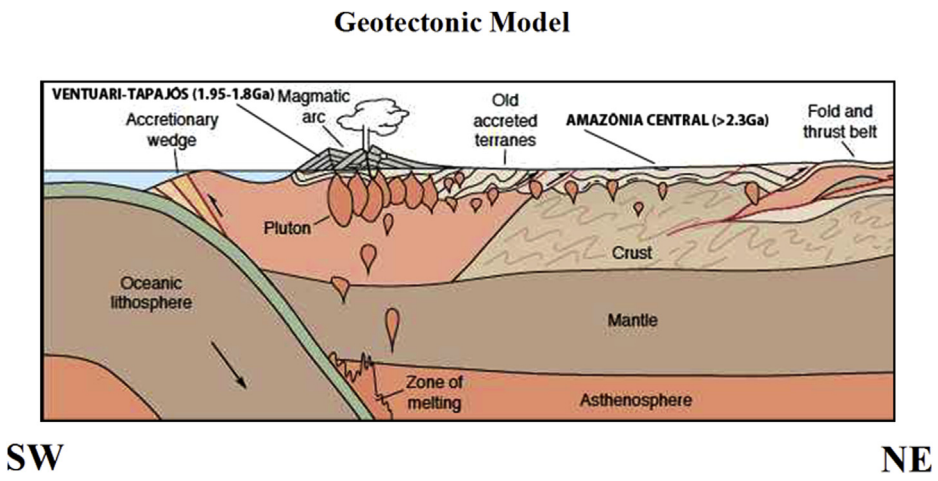

Fig. 13. Proposed Geotectonic Model for the study area (adapted from Hamblin and Christiansen, 1998; and from Valério et al., 2006).

obtained the same direction for two seismological stations located in French Guyana (Fig. 12), we are tempted to conclude that, for the Guyana shield, the symmetry axis directions of the measured anisotropy seem to show the prevailing direction of the crustal structure (Table 1). It is also interesting that the anisotropy direction observed for the JABU station, located near Manaus, in the middle of the Amazon basin (Fig. 12), in an area covered with more than 2000 m of Phanerozoic sedimentary rock layers (Almeida et al., 1978), shows the same direction as the other stations located on the exposed shield area. This may indicate that both the continuing Guyana shield trends underneath the Amazon basin, and point to the consistency of the SKS shear wave results of Krüger et al. (2002). On the other hand, Assumpção et al. (2011) obtained an almost E–W prevailing direction on a measurement made at the SNVB station (Fig. 12, Table 1).

Considering the sudden change of the observed main trend of the magnetic anomalies on the border (approximately N110E border, marked as the orange dashed line of Fig. 5) separating the Ventuari-Tapajós on the west from the Amazônia Central geochronological provinces, we have an additional element for the interpretation of the main Proterozoic trends observed on the Guyana shield (Fig. 12).

So, based on the main direction of the magnetic anomalies on Proterozoic provinces identified in the area, on the available geological surface geology mapping, it may be possible to propose a geotectonic model for the region. This would include the origin and evolution of the Proterozoic terrains of the study area (Fig. 13), in a similar way to the original idea of Valério et al. (2006), with the location of the former subduction zone, as well as the corresponding accretionary terrains as shown on Fig. 13. The proposed model includes the past Amazônia Central continental plate (>2.3 Ga), as well as the accreted terrains of the Ventuari-Tapajós province (1.95–1.80 Ga, according to Valério et al., 2009). In this case, the nature of the measured anisotropy on the Guyana shield may be related to the changes on imprinted magnetic structures, formerly parallel to the past collision front, thus reflecting the Proterozoic tectonic events, frozen-in on the lithosphere.

7. Conclusions

Digital image processing of aerogeophysical data may add to the knowledge on the geologic structure of the southern portion of the Guyana shield in Brazil. The geophysical data were processed using spatial data integration strategy on a fine interpolated mesh, which yielded high resolution images, correlated to the local surface geologic units. The joint analysis of the resulting stacked images enabled correlation with the existing geological information on a laterally continuous environment, enhancing the ability to interpret regional geological changes observed in the study area of the Amazonian craton.

The main geochronological provinces and geologic formations previously known to the researched area were identified both from the treated aeromagnetic and radiometric images. The border limiting the Amazonia Central (>2.3 Ga), and the Ventuari-Tapajós (1.95–1.80 Ga) provinces, defined from the processing of the aeromagnetic images, follows the valley of the Uatumã river in the study area. This limit separates magnetic anomalies trending EW, associated to the Ventuari-Tapajós province (eastern, central and northern sectors of the study area), from magnetic anomalies trending approximately N120E, corresponding to the Amazonia Central province (observed in the southwestern corner of the area).

On a regional scale, it was possible to examine the available information on the main trends of Proterozoic geologic structures, specially the greenstone belt alignments, and to consider the distribution of measured SKS shear-wave splitting direction. From that analysis, it is possible to identify a parallelism between these features and the direction of the borders limiting the Proterozoic geochronological provinces of the Amazonian craton on the southern Guyana shield.

Finally, based on the parallelism among mapped geochronological provinces of the Amazonian craton, and observed geophysical structures and trends on the study area, a Proterozoic geotectonic model is proposed for the southern Guyana shield. The model includes the past Amazônia Central former continental plate, and the accreted terrains of the Ventuari-Tapajós province.

Acknowledgments

We thank V. Souza and H. T. Costi for sharing geologic information about the area with us. We also thank the Brazilian Geologic Service, CPRM, especially Mr. L. M. F. Mourão and Mrs. M. L. V. de Azevedo, for providing us with the most valued aerogeophysical data. L. Gee, G. Barruol, R. Dall'Agnoll, and an anonymous reviewer, provided valuable comments that enriched the original draft of this paper. We thank the Pitinga Mine Company colleagues for providing us with the necessary field support for maintaining the Pitinga station. We are grateful to the agreement among the University of Brasília and the Santo Antônio Energia S.A. power company (Agreement FUB-SAE). R. Fuck acknowledges CNPq (grant 30.3341/2011-4) for field and laboratory support.

References

Almeida, F.F.M., Martin, C., Ferreira, E.O., Furque, G., 1978. Tectonic map of South America, scale 1:5.000.000. DNPM-CGMW-UNESCO, Brasília.

Almeida, F.F.M., Brito Neves, B.B., Carneiro, C.D.R., 2000. The origin and evolution of the South American Platform. Earth-Sci. Rev. 50 (1–2), 77–111. http://dx.doi.org/10.1016/S0012-8252(99)00072-0.

Almeida, M.E., 2006. Evolução geológica da porção centro-sul do escudo das Guianas com base no estudo geoquímico, geocronológico (evaporação de Pb e U-Pb ID-TIMS em zircã o) e isotópico (Nd-Pb) dos granitóides Paleoproterozóicos do sudeste de Roraima. Tese de Doutorado. Universidade Federal do Pará, Instituto de Geociências, Belém, p. 227.

Almeida, J.A.C., Guimarães, F.V., Dall'Agnol, R., 2007. Petrologia magnética do granito anorogênico Bannach, Terreno Granito-Greenstone de Rio Maria, Pará. Rev. Bras. Geociências 37, 17–36.

Almeida, J.A.C., Oliveira, M.A., Dall'Agnol, R., Leite, A.A.S., Althoff, F.J., 2008. Mesoarchean tonalite-trondhjemite-granodiorite (TTG) associations of the Rio Maria Granite-Greenstone Terrane, Amazonian craton. In: International Geological Congress, 2008, Oslo, 33 International Geological Congress.

Araújo Neto, H., Moreira, H.L., 1976. Projeto Estanho de Abonari. Brasília, MME/DNPM/CPRM. Relatório 1, 232.

Assumpção, M., Guarido, M., van der Lee, S., Dourado, J.C., 2011. Upper-mantle seismic anisotropy from SKS splitting in the South American stable platform: a test of asthenospheric flow models beneath the lithosphere. Lithosphere 3 (2), 173–180. http://dx.doi.org/10.1130/L99.1.

Barruol, G., Hoffmann, R., 1999. Upper mantle anisotropy beneath the goescope stations. J. Geophys. Res. 104, 10,757–10,774. http://dx.doi.org/10.1029/1999JB900033.

Barruol, G., Silver, P.G., Vauchez, A., 1997. Seismic anisotropy in the eastern United States: deep structure of a complex continental plate. J. Geophys. Res. 102, 8329–8348. http://dx.doi.org/10.1029/96JB03800.

Bastos Neto, A.C., Pereira, V.P., Ronchi, L.H., Lima, E.F., Frantz, J.C., 2009. The world-class Sn, Nb, Ta, F (Y, REE, Li) deposit and the massive cryolite associated with the albite-enriched facies of the Madeira A-type granite, Pitinga mining district, Amazonas state, Brazil. Can. Mineral. 47, 1329–1357. http://dx.doi.org/10.3749/canmin.47.6.1329.

Bizzi, L.A., Schobbenhaus, C., Vidotti, R.M., Gonçalves, J.H. (Eds.), 2003. Geologia, Tectônica e Recursos Minerais do Brasil. CPRM, Ed. UnB, Brasília.

Bokelmann, G.H.R., Wüstefeld, A., 2009. Comparing crustal and mantle fabric from the North American craton using magnetics and seismic anisotropy. Earth Planet. Sci. Lett. 277 (3–4), 355–364. http://dx.doi.org/10.1016/j.epsl.2008.10.032.

Brito Neves, B.B., Almeida, F.F.M., 2003. A evolução dos crátons Amazônico e São Francisco comparada com homólogos no hemisfério norte – 25 anos depois. In: 8° Simpósio de Geologia da Amazônia. SBG-NO, Manaus, AM.

Bungum, H., Pirhonen, S.E., Husebye, E.S., 1980. Crustal thicknesses in Fennoscandia. Geophys. J. Royal Astron. Soc. 63, 759–774. http://dx.doi.org/10.1111/j.1365-246X.1980.tb02650.x.

Costi, H.T., 2000. Petrologia de granites alcalinos com alto flúor mineralizados em metais raros: o exemplo do albita-granito da mina Pitinga, Amazonas, Brasil. Doctorate thesis. Universidade Federal do Pará, Belém, Brazil, 345p.

Costi, H.T., Dall'Agnol, R., Moura, C.A.V., 2000. Geology and Pb-Pb geochronology of paleoproterozoic volcanic and granitic rocks of the Pitinga Province, northern Brazil. Int. Geol. Rev. 42, 832–849. http://dx.doi.org/10.1080/00206810009465114.

Costi, H.T., Dall'Agnol, R., Pichavant, M., Rämö, O.T., 2009. The peralkaline tin-mineralized Madeira cryolite albite-rich granite of Pitinga, Amazonian craton, Brazil: petrography, Mineralogy, and crystallization processes. Can. Mineral. 47, 1301–1327. http://dx.doi.org/10.3749/canmin.47.6.1301.

CPRM, 2007. Projeto Aerogeofísico Pitinga. Texto Técnico. In: Programa Geologia do Brasil (PGB), vol. I. Min. Minas Energ., Brasília.

Ernst, W.G., 2009. Archean plate tectonics, rise of proterozoic supercontinentality and onset of regional episodic stagnant-lid behavior. Gondwana Res. 15 (3–4), 243–253. http://dx.doi.org/10.1016/j.gr.2008.06.010.

Fairhead, J.D., Maus, S., 2003. CHAMP satellite and terrestrial magnetic data help refine the tectonic model for South America and resolve the lingering problem of the pre-break-up fit of the South Atlantic Ocean. Lead. Edge 22 (8), 779–783.

Ferron, J.M.T.M., 2006. Geologia regional, geoquímica e geocronologia Pb-Pb de rochas graníticas e vulcânicas paleoproterozóicas da Província Pitinga, craton amazônia. Tese de Doutorado. Instituto de Geociências. Universidade Federal do Rio Grande do Sul, Porto Alegre, 331pp. URI. http://hdl.handle.net/10183/8529.

Ferron, J.M.T.M., Bastos Neto, A.C., Lima, E.F., Costi, H.T., Moura, C.A.V., Prado, M., Pierosan, R., Galarza, M.A., 2006. Geologia e geocronologia Pb-Pb de rochas graníticas e vulcânicas ácidas a intermediárias Paleoproterozóicas da Província Pitinga, Cráton Amazônico. Rev. Bras. Geociências 36 (3), 499–512.

Ferron, J.M.T.M., Bastos Neto, A.C., Lima, E.F., Nardi, L.V.S., Costi, H.T., Pierosan, R., Prado, M., 2010. Petrology, geochemistry, and geochronology of Paleoproterozoic volcanic and granitic rocks (1.89 to 1.88 Ga) of the Pitinga Province, Amazonian craton, Brazil. J. South Am. Earth Sci. 29, 483–497. http://dx.doi.org/10.1016/j.jsames.2009.05.001.

Fraga, L.M.B., 2002. A associação Anortosito-Mangerito-Granito Rapakivi (AMG) do cinturão Guiana Central, Roraima e suas encaixantes paleoproterozóicas: evolução estrutural, geocronologia e petrologia. Tese de Doutorado. CPGG/CG, Universidade Federal do Pará, Belém, p. 386.

Fraga, L.M., Dall'Agnol, R., Costa, J.B.S., Macambira, M.J.B., 2009a. The Mesoproterozoic Mucajaí anorthosite-mangerite-rapakivi granite association, Amazonian craton, Brazil. Can. Mineral. 47, 1469–1492. http://dx.doi.org/10.3749/canmin.47.6.1469.

Fraga, L.M., Macambira, M.J.B., Dall'Agnol, R., Costa, J.B.S., 2009b. 1.94 1.93 Ga charnockitic magmatism from the central part of the Guyana shield, Roraima, Brazil: single-zircon evaporation data and tectonic implications. J. South Am. Earth Sci. 29, 247–257. http://dx.doi.org/10.1016/j.jsames.2009.02.007.

Fuck, R.A., Pimentel, M.M., Machado, N., Daoud, W.E.K., 1993. Idade U-Pb do Granito Madeira, Pitinga (AM). In: Boletim de Resumos Expandidos do 4° Congresso Brasileiro de Geoquímica, Brasília, pp. 246–249.

Geosoft, 2010. Oasis Montaj 7.2 Mapping and Processing System Manual. Geosoft Inc., Toronto.

Grand, S.P., Helmberger, D.V., 1984. Upper mantle shear structure of North America. Geophys. J. Royal Astron. Soc. 76, 399–438. http://dx.doi.org/10.1111/j.1365-246X.1984.tb05053.x.

Hamblin, W.K., Christiansen, E.H., 1998. Earth's dynamic systems. Prentice-Hall, 740 pp.

IAEA, 1991. Airborne Gamma Ray Spectrometer Surveying. International Atomic Energy Agency, Vienna, Austria. Technical Reports Series No. 323.

IAEA, 2003. Guidelines for Radioelement Mapping Using Gamma Ray Spectrometry Data. International Atomic Energy Agency, Vienna, Austria. TECDOC-1363.

Ivan, M., Silva, L.J.H.D., Marza, V., 2001. Probing the subcontinental South American upper mantle with SKS splitting at some selected Brazilian sites. Rev. Roum. Géophysique 45, 39–57.

James, D.E., Assumpção, M., Snoke, J.A., Ribotta, L.C., Kuehnel, R., 1993. Seismic studies of continental lithosphere beneath SE Brazil. An. Acad. Bras. Ciências. ISSN: 0001-3765 65, 227–250.

Journel, A.G., Huijbregts, C.J., 1978. Mining Geostatistics. Academic Press, New York, p. 600.

Kennett, B.L.N., Engdahl, E.R., 1990. Traveltimes for global earthquake location and phase identification. Geophys. J. Int. 105, 429–465. http://dx.doi.org/10.1111/j.1365-246X.1991.tb06724.x.

Kind, R., Vinnik, L.P., 1988. The upper mantle discontinuities underneath the GRF array from P- to-S converted phases. J. Geophys. 62, 138–147.

Krüger, F., Scherbaum, F., Rosa, J.W.C., Kind, R., Zetsche, F., Höhne, J., 2002. Crustal and upper mantle structure in the Amazon region (Brazil) determined with broadband mobile stations. J. Geophys. Res. 107 (B10), 2265–2277. http://dx.doi.org/10.1029/2001JB000598.

Lamarão, C.N., Dall'Agnol, R., Lafon, J.M., Lima, E.F., 2002. Geology, geochemistry and Pb-Pb zircon geochronology of the paleoproterozoic magmatism of Vila Riozinho, Tapajós Gold Province, Brazil. Precambrian Res. 119 (1–4), 189–223. http://dx.doi.org/10.1016/S0301-9268(02)00123-7.

Lamarão, C.N., Dall'Agnol, R., Pimentel, M.M., 2005. Nd isotopic composition of Paleoproterozoic volcanic and granitoid rocks of Vila Riozinho: implications for the crustal evolution of the Tapajós Gold Province, Amazon craton. J. South Am. Earth Sci. 18, 277–292. http://dx.doi.org/10.1016/j.jsames.2004.11.005.

Langston, C.A., 1977. The effect of planar dipping structures on source and receiver responses for constant ray parameter. Bull. Seismol. Soc. Am. 67, 1029–1050 doi:10.1.1.128.7468.

Langston, C.A., 1979. Structure under Mount Rainier, Washington, inferred from teleseismic body waves. J. Geophys. Res. 84, 4749–4762. http://dx.doi.org/10.1029/JB084iB09p04749.

Lloyd, S., van der Lee, S., França, G.S., Assumpção, M., 2010. Moho map of South America from receiver functions and surface waves. J. Geophys. Res. 115, B11315. http://dx.doi.org/10.1029/2009JB006829.

Luyendyk, A.P.J., 1997. Processing of airborne magnetic data. AGSO J. Aust. Geology Geophys. 17 (2), 31–38.

Maus, S., Sazonova, T., Hemant, K., Fairhead, J.D., Ravat, D., 2007. National geophysical data center candidate for the world digital magnetic anomaly map. Geochem. Geophys. Geosyst. 8. http://dx.doi.org/10.1029/2007GC001643.

McReath, I., Faraco, M.T.L., 2006. Paleoproterozoic greenstone-granite belts in northern Brazil and the former Guyana shield-west African craton province. Rev. do Inst. Geociências – USP 5 (2), 49–63. http://dx.doi.org/10.1590/S1519-874X2006000100004.

Mooney, W.D., Laske, G., Masters, T.G., 1998. CRUST 5.1: a global crustal model at 5 degrees × 5 degrees. J. Geophys. Res. 103, 727–747. http://dx.doi.org/10.1029/97JB02122.

Prothero, D.R., Dott Jr., R.H., 2009. Evolution of the Earth, eighth ed. McGraw-Hill Science and Engineering, p. 576.

Reis, N.J., Fraga, L.M., Faria, M.S.G., Almeida, M.E., 2003. Geologia do Estado de Roraima, Brasil. In: Rossi, F., Jean-Michel, L., Vasquez, M.L. (Eds.), Geology of France and Surrounding Areas, vols. 2–4. Ed. Brgm, Paris, France, pp. 121–134.

Rosa, J.W.C., 1993. Regional seismicity of the Amazon Region and the new proposed digital station in Brazil. Fifth Annual IRIS Workshop, Waikoloa, Hawaii, USA.

Rosa, J.W.C., Rosa, J.W.C., Fuck, R.A., 2012. Crust and upper mantle structure in central Brazil derived by receiver functions and SKS splitting analysis. J. South Am. Earth Sci. 34, 33–46. http://dx.doi.org/10.1016/j.jsames.2011.09.001.

Santos, J.O.S., Silva, L.C., Faria, M.S.G., Macambira, M.J.B., 1997. Pb-Pb single crystal, evaporation isotopic study on the post-tectonic, sub-alkalic, A-type Moderna granite (Mapuera Intrusive Suite), State of Roraima, northern Brazil. In: Ferreira, V.P., Sial, A.N. (Eds.), International Symposium on Granites and Associated Mineralizations, 2, Salvador, Brazil. Superintendência de Geologia e Recursos Minerais, Governo do Estado da Bahia, Extended Abstracts and Program, 273–275.

Santos, J.O.S., Hartmann, L.A., Gaudette, H.E., Groves, D.I., McNaughton, N.J., Fletcher, I.R., 2000. A new understanding of the provinces of the Amazon craton based on integration of field mapping, and U-Pb and Sm-Nd geochronologym. Gondwana Res. 3 (4), 453–488. http://dx.doi.org/10.1016/S1342-937X(05)70755-3.

Santos, J.O.S., Groves, D.J., Hartmann, L.A., Moura, M.A., McNaughton, N.J., 2001. Gold deposits of the Tapajós and Alta Floresta Domains, Tapajós-Parima orogenic belt, Amazon craton, Brazil. Miner. Deposita 36, 278–299. http://dx.doi.org/10.1007/s001260100172.

Santos, J.O.S., Hartmann, L.A., McNaughton, N.J., Fletcher, I.R., 2002. Timing of mafic magmatism in the Tapajós Province (Brazil) and implications for the evolution of the Amazon Craton: evidence from baddeleyite and zircon U-Pb SHRIMP geochronology. J. South Am. Earth Sci. 15 (4), 409–429. http://dx.doi.org/10.1016/S0895-9811(02)00061-5.

Santos, J.O.S., 2003. Geotectônica dos Escudos das Guianas e Brasil-Central. In: Bizzi, L.A., Schobbenhaus, C., Vidotti, R.M., Gonçalves, J.H. (Eds.), Geologia, Tectônica e Recursos Minerais do Brasil (texto, mapas & SIG). Serviço Geológico do Brasil – CPRM/MME, Brasília, pp. 169–226.

Santos, J.O.S., Van Breemen, O.B., Groves, D.I., Hartmann, L.A., Almeida, M.E., McNaughton, N.J., Fletcher, I.R., 2004. Timing and evolution of multiple Paleoproterozoic magmatic arcs in the Tapajós Domain, Amazon craton: constraints from SHRIMP and TIMS zircon, baddeleyite and titanite U-Pb geochronology. Precambrian Res. 131, 73–109. http://dx.doi.org/10.1016/j.precamres.2004.01.002.

Santos, J.O.S., Hartmann, L.A., Faria, M.S.G., Ricker, S.R., Souza, M.M., Almeida, M.E., McNaughton, N.J., 2006. A compartimentação do Cráton Amazonas em províncias: avanços ocorridos no período 2000–2006. In: SBG-NO, Simpósio de Geologia da Amazônia, 9. CD-ROM, Belém.

Silver, P.G., Kaneshima, S., 1993. Constrains on mantle anisotropy beneath Precambrian North America from transportable experiment. Geophys. Res. Lett. 20, 1127–1130. http://dx.doi.org/10.1029/93GL00775.

Silver, P.G., 1996. Seismic anisotropy beneath the continents: probing the depths of geology. Annu. Rev. Earth Planet. Sci. 24, 385–432. http://dx.doi.org/10.1146/annurev.earth.24.1.385.

Sleep, N.H., Windley, B.F., 1982. Archean plate tectonics: constraints and inferences. J. Geology 90 (4), 363–397. http://dx.doi.org/10.1086/628691.

Souza, V.S., Nogueira, A.C.R., 2009. Seção geológica Manaus-Presidente Figueiredo (AM), borda norte da Bacia do Amazonas: um guia para excursão de campo. Rev. Bras. Geociências 39 (1), 16–29.

Tassinari, C.C.G., Macambira, M.J.B., 1999. Geochronological provinces of the Amazonian Craton. Episodes 22 (3), 174–182.

Tassinari, C.C.G., Bettencourt, J.S., Geraldes, M.C., Macambira, M.J.B., Lafon, J.M., 2000. The Amazonian craton. In: Cordani, U.G., Milani, E.J., Thomaz Filho, A., Campos, D.A. (Eds.), Tectonic Evolution of South America, 31st Inter. Geol. Congr.,. Ed. FINEP/CT PETRO, Rio de Janeiro, pp. 41–95.

Tassinari, C.C.G., Macambira, M.J.B., 2004. A evolução tectônica do Cráton Amazônico. In: Mantesso-Neto, V., Bartorelli, A., Dal Ré Carneiro, C., Brito-Neves, B.B. (Eds.), Geologia do Continente Sul-Americano: Evolução da obra de Fernando Flávio Marques de Almeida. Ed. Beca, São Paulo, pp. 471–485.

Valério, C.S., Souza, V.S., Macambira, M.J.B., Milliotti, C.A., Carvalho, A.S., 2005. Geoquímica e idade Pb-Pb de zircão do Grupo Iricoumé na região da borda norte da bacia do Amazonas, município de Presidente Figueiredo (AM). In: SBG, Simp. Vulc. Amb. Assoc.. Anais, vol. 3, pp. 47–52.

Valério, C.S., Souza, V.S., Macambira, M.J.B., Galarza, M.A., 2006. Geoquímica e geocronologia Pb-Pb da Suíte Intrusiva Água Branca, Município de Presidente Figueiredo (AM): evidência de colisão no Paleoproterozóico da Amazônia Ocidental. Rev. Bras. Geociências 36 (2), 359–370. ISSN RBG online 2177–4382.

Valério, C.S., Souza, V.S., Macambira, M.J.B., 2009. The 1.90-1.88 Ga magmatism in the southernmost Guyana Shield, Amazonas, Brazil: geology, geochemistry, zircon geochronology, and tectonic implications. J. South Am. Earth Sci. 28, 304–320. http://dx.doi.org/10.1016/j.jsames.2009.04.001.

Valério, C.S., Macambira, M.J.B., Souza, V.S., 2012. Field and petrographic data of 1.90 to 1.88 Ga I- and A-type granitoids from the central region of the Amazonian Craton, NE Amazonas State, Brasil. Rev. Bras. Geociências 42 (4), 690–712. http://dx.doi.org/10.5327/Z0375-75362012000400004.

Van Kranendonk, M.J., 2010. Two types of Archean continental crust: plume and plate tectonics on early Earth. Am. J. Sci. 310 (10), 1187–1209. http://dx.doi.org/10.2475/10.2010.01.

Veiga Jr., J.P., Nunes, A.C.B., Fernández, A.S., Amaral, J.A.F., Amaral, J.E., Pessoa, M.R., Cruz, S.A.S., 1979. Projeto Sulfetos do Uatumã. DNPM-CPRM, Manaus, Brasil (7 vols.).

Vinnik, L.P., 1977. Detection of waves converted from P to SV in the mantle. Phys. Earth Planet. Interiors 15, 39–45. http://dx.doi.org/10.1016/0031-9201(77)90008-5.

Vinnik, L.P., Makeyeva, L.I., Milev, A., Usenko, A.Y., 1992. Global patterns of azimuthal anisotropy and deformations in the continental mantle. Geophys. J. Int. 111, 433–447. http://dx.doi.org/10.1111/j.1365-246X.1992.tb02102.x.

Wüstefeld, A., Bokelmann, G., Barruol, G., 2010. Evidence for ancient lithospheric deformation in the East European craton based on mantle seismic anisotropy and crustal magnetics. Tectonophysics 481, 16–28. http://dx.doi.org/10.1016/j.tecto.2009.01.010.

Yuan, X., Ni, J., Kind, R., Mechie, J., Sandvol, E., 1997. Lithospheric and upper mantle structure of shouthern Tibet from a seismological passive source experiment. J. Geophys. Res. 102, 27491–27500. http://dx.doi.org/10.1029/97JB02379.

Zhu, L., Kanamori, H., 2000. Moho depth variation in southern California from teleseismic receiver functions. J. Geophys. Res. 105, 2969–2980. http://dx.doi.org/10.1029/1999JB900322.